atmosphere

Article

Understanding the Susceptibility of the Tropical Proglacial Environment in Peru Using Optical Imagery and Radon Measurements

Diego Antonio García-Tadeo [1,2,3,4,*], Modesto Montoya-Zavaleta [5] and Yumin Tan [1]

[1] School of Transportation Science and Engineering, Beihang University, No. 37 Xueyuan Road, Haidian District, Beijing 100191, China
[2] Graduate School of Civil Engineering, Universidad Nacional de Ingeniería, Av. Túpac Amaru 210, Lima 15333, Peru
[3] National Institute for Research on Glaciers and Mountain Ecosystems (INAIGEM), Ministry of the Environment (MINAM), Av. Centenario 2656, Huaraz 02002, Peru
[4] Department of Civil Engineering, Universidad Nacional Santiago Antúnez de Mayolo, Av. Centenario 200, Huaraz 02002, Peru
[5] Graduate School of Science, Universidad Nacional de Ingeniería, Av. Túpac Amaru 210, Lima 15333, Peru
* Correspondence: dgarciat@unasam.edu.pe

Abstract: The tropical glaciers of the Cordillera Blanca have played host to some of the most significant mass movements ever recorded in the world and Peru; many proglacial lakes formed in this mountain range have natural dikes made of moraine material, which, if they collapse, would present a risk for the cities located downstream of a proglacial lake, where the proglacial lake Palcacocha has a remarkable background regarding floods. The Sentinel-2 MSI (Multi-Spectral Instrument, Level-2A) has a specific band for snow probability mapping that indicates glaciers and snow cover; this is effective for recognizing proglacial lakes by calculating the $NDWI_{ice}$. It is also helpful for lithology with *SWIR* for granite moraine deposits and slate moraines in the proglacial environment Palcacocha; these deposits surround the proglacial lake, with $NDWI_{ice}$ determining the perimeter where sediment interacts with the rocks and meltwater. In addition, there are high radon concentrations made by ice avalanche impacts on the proglacial lake. Unstable glacier blocks cause ice avalanches into this proglacial lake, and the radon responds to flow variations from these high-impact avalanches. We used the device RadonEye PLus2, which allows real-time detection of radon flux changes in the proglacial environment. Our results indicated that ice avalanches making a high impact in the proglacial lake cause turbulent flow and generate radon concentration marks with a rising magnitude, while the absence of ice avalanches in the lake will cause the values to go down. The relationships of radon concentrations in the atmosphere for a tropical proglacial environment are radon and temperature ($R^2 = 0.364$), radon and humidity ($R^2 = 0.469$). In a passive proglacial environment with prolonged rainfall, radon concentrations tend to decrease, with an inversely proportional relationship between humidity and radon in the tropical proglacial environment. Proglacial lakes in the tropical zone often have large volumes of freshwater with high slopes from tropical glaciers, and climate change effects are an imminent danger for nearby cities.

Keywords: tropical glacier; proglacial environment; remote sensing; radon; Peru

Citation: García-Tadeo, D.A.; Montoya-Zavaleta, M.; Tan, Y. Understanding the Susceptibility of the Tropical Proglacial Environment in Peru Using Optical Imagery and Radon Measurements. *Atmosphere* **2023**, *14*, 568. https://doi.org/10.3390/atmos14030568

Academic Editor: Cucoş (Dinu) Alexandra

Received: 8 February 2023
Revised: 10 March 2023
Accepted: 13 March 2023
Published: 16 March 2023

1. Introduction

A glacier is a mass of snow, recrystallized ice, and pieces of rock that accumulate in large quantities, which is what forms proglacial lakes [1]. Since tropical glaciers generate glacier mass impacts in nearby proglacial lakes, and since the radon decomposes and produces an alpha form of ionizing radiation [2] which is also used for natural hazards, the analyzed for preventing GLOFs is open, then respective analysis with the proglacial tropical environment is imminent. The radon atom moves in the proglacial lake periphery, water that has recently come into direct contact with sediment or bedrock containing radon [3], geochemical composition in nearby areas of glaciers that includes outwash deposits and derived soils can closely compare with local bedrock units and as such allows potential radon assessments [4]; radon's diffusive flux from channel floor sediments of the proglacial environment has a potential source of radon, particularly after the onset of widespread melting across the catchment and development of a channelized system [5] and at the moment when gusts increase, concentrations of radon decrease [6,7]. On the contrary, when temperatures increase, radon levels rise [8,9].

Glacier and sediment-related hazards in a proglacial environment are typical, and if the scenario is a temperature that tends to increase, it causes rapid melting of glaciers and hazards such as glacial lake outbursts [10]. In the last few decades, many far-flung satellites with diverse sensors were launched into Earth's orbit with specific objectives for the cryosphere, which means that we can estimate snow coverage via remote sensing. In particular, some of this satellite data are publicly available and completely free; as an example, Sentinel-2 satellites can offer multi-spectral imagery with a 10-m resolution and a 5-day global revisit frequency for spatial-temporal land floor monitoring [11]. One of the most difficult parts of snow coverage mapping via satellite imagery is distinguishing snow from a cloud. The biggest problem is that snow and cloud cover look very similar and have even color distribution, and manually isolating snow pixels from cloud pixels requires expert information supplemented by field measurements [12]. To detect proglacial environments, Sentinel-2 makes optical imagery from specific bands; band 20 has a higher resolution of its data that helps to identify snow and glaciers for inventorying [13]. For proglacial lakes, the calculation of *NDWI* with Sentinel-2 is a useful tool since it is used to monitor changes related to water content in water bodies [14]. Currently, there are several threshold test-based tools that are good for classifying clouds, cirrus, snow and shadows [15], and optical remote sensing over the snow-covered ground for a cryosphere where meltwater from glaciers is translucent [16]. Meltwater from glaciers makes a complement with radon measurements; there are many methods, such as groundwater discharge to wetlands driven by storm and flood events for quantification using continuous Radon-222 [17]. A study about radon and ground radioactivity shows that radon air concentrations increase more and more during floods [18]; another study about flooding and radon was done in Tonle Sap Lake in Cambodia, analyzing a flood system with a review of radon results [19]. In Peru, when measuring radon in soils, high radon concentrations were found in cases of maximum river flooding that was associated with ground vibrations caused by rock and debris avalanches on the rivers [20].

Based on our analysis, it is necessary to study radon in tropical zones where proglacial lakes exist and shows analyses that correspond to the impacts of climate change in tropical proglacial environments. We spotted a problem in the introduced methods: Not taking tropical proglacial lakes with radon and ignoring direct sources like the optical imagery with specific bands (band 20) from Sentinel-2 satellite images that have scenes including representative glaciers with snow cover and backgrounds that are distributed in the tropical zone, the measurements of radon are focused in variations in tropical proglacial environment that generate high concentrations of radon from the susceptibility when tropical glaciers are impacted by ice avalanches and generate meltwater turbulence that tends to cause a proglacial lake to outburst. At that point, it is necessary to know how to prevent ice avalanches that can generate GLOF.

2. Study Area

2.1. Tropical Zone

Peru has 70% of Earth's tropical glaciers and is an important source of meltwater for domestic consumption, hydropower generation, and agriculture [21]. Furthermore, the mountain ranges of Peru that have tropical glaciers are important indicators to show the effects of climate change, such as the case of the Cordillera Blanca which presents a high discharge of meltwater [22]. The tropical glaciers of Cordillera Blanca have a crucial impact on meltwater runoff [23], which has created many proglacial lakes, and the proglacial lake Palcacocha has the suitable characteristics for studying GLOFs [24].

Tropical glaciers are found between the Tropic of Cancer and the Tropic of Capricorn, which are impacted by climate change, increasing the water volumes of many proglacial lakes; Peru has the largest area of tropical glaciers in the world [25], grouped in the mountain ranges shown in Figure 1.

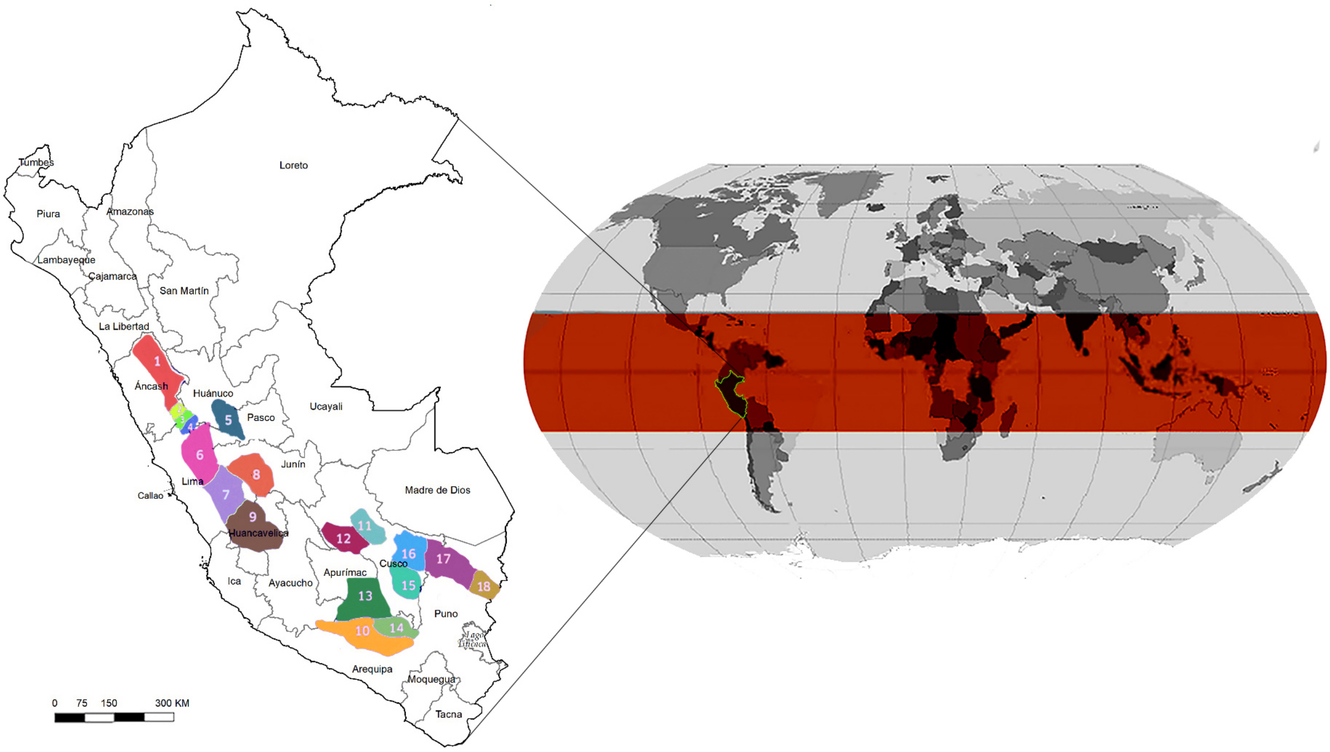

Figure 1. The tropical zone is shown in the red stripe, where Peru has glaciated areas inside mountain ranges.

Regarding climate change, the receding of the Peruvian glaciers has a significant impact on the ecosystem and communities [26]; if glacier runoff decreases over time, many glaciers will be lost [27] and glacial mountain ranges will disappear due to the effects of climate change, and Peru has already lost 51% of its glacier surface in the last 50 years. Table 1 shows the mountain ranges that have glaciated areas.

Glacier mass loss rates are particularly concerning in the tropics, where changes in glacier meltwater fluxes pose serious risks to downstream communities [28]. The Cordillera Blanca is the heaviest glacierized tropical range in the world and many glaciers have melted recently [29]. The melting is largely due to climate change, which is generating new proglacial lakes in the Cordillera Blanca and increasing the volume of water in the existing ones via runoff [30]. Unsteady or unreliable water runoff is known to cause hazardous GLOF in many scenarios, and also causes several socio-economic issues [31]. In addition, glacial retreat rapidly leads to large flows [32] which threaten downstream areas due to their potential to cause many floods or to further melt tropical glaciers.

Table 1. Percentage of glaciated area in mountain ranges of Peru.

Code	Label	Percentage of Glaciated Area	Name
1		40.63%	Cordillera Blanca
2		0.54%	Codillera Huallanca
3		4.26%	Cordillera Huayhuash
4		2.18%	Cordillera Raura
5		0.75%	Cordillera Huagaruncho
6		0.46%	Cordillera La Viuda
7		4.00%	Cordillera Central
8		2.03%	Cordillera Huaytapallana
9		0.11%	Cordillera de Chonta
10		4.69%	Cordillera Ampato
11		2.03%	Cordillera Urubamba
12		9.95%	Cordillera de Huanzo
13		0.35%	Cordillera de Vilcabamba
14		0.07%	Cordillera Chila
15		0.24%	Cordillera La Raya
16		21.52%	Cordillera de Vilcanota
17		2.66%	Cordillera de Carabaya
18		3.48%	Cordillera Apolobamba

2.2. Proglacial Lakes with Potential to Cause GLOFs

Proglacial lakes form in front of glaciers, usually as a result of glacier retreats. In front of a surviving glacier, the proglacial lake occupies the central part of the glacial depression, from the glacier upstream to a frontal moraine. When glaciers have been thawing for a long time, the proglacial lake occupies the part of the depression set between two old frontal moraines. A glacier is a mass of ice that forms on the Earth's surface. Far from standing still, glaciers move little by little, due to the slope and the impact of climate change. Moraines are the materials, mainly rock fragments, that the ice pulls up and drags. They accumulate in various parts of the frozen mass: sides, front, terminus, and bottom. Proglacial lakes originate when the water occupies the depression created by the receding ice. The phenomenon, known as GLOF, happens for many reasons, the most common of which are a big mass of ice impacting the proglacial lake, an avalanche of ice, or if the moraine that closes the glacial lake gives way to the pressure of the accumulated water.

This type of event has 3 main characteristics:

- A sudden release of water.
- Happens very quickly.
- Rising waters lead to large downstream discharges.

However, in recent years, the risk has increased markedly. Thus, an analysis of satellite images carried out in 2020 revealed that the number of glacial lakes had increased during the period 1990–2018 [33], mainly due to climate change which is causing the rapid melting of the glaciers. Climate change generates new proglacial lakes and causes existing ones to increase their volume, which leads to a risk of flooding in nearby areas.

To establish whether a proglacial lake should be considered capable of generating significant vulnerability for people, it must be determined if there are populations and infrastructure downstream, which in the GLOF event may be in the water channel, and if the volume of water contained by the proglacial lake is uncontainable. It is also important if there are unstable slopes, glaciers or amounts of loose material above the lagoon which can fall into the water and cause a wave strong enough to break or exceed the moraine of the proglacial lake, which is fundamental to knowing how stable the moraine is. The hazard from GLOF from an unstable moraine or ice avalanche is dangerous to people living close to the glacier and in the valley, including many tourists, since the warning time for such an event may only be a minute or so for people at the terminus and even less for people close to the glacier. This, therefore, represents a not insignificant threat to people's safety [34]. The Cordillera Blanca is frequented by tourists, concentrating a large number of people in a small area, in addition to the residents, which is why knowledge of the GLOFs is very important. The tropical glacial melt on the order of 15–18 m per year since the 1980s in Peru's Cordillera Blanca is an example of how we must improve important technical support for Disaster Risk Management [35]. Disaster risk management is understood as the systematic process that integrates the definition, prevention, mitigation and transfer of risk, as well as disaster preparedness, emergency response and rehabilitation and reconstruction, in order to mitigate the disaster impacts (UNISDR, 2004). This definition presents two essential ideas: first, that risk management is a process and not an ultimate goal of the disaster that has already materialized, and second, that risk management is carried out both to reduce the existing risk and to avoid the generation of new risks. These two essential ideas have been materialized in the Sendai Framework for Disaster Risk Reduction 2015–2030 (Sendai Framework).

2.3. Proglacial Environment

Proglacial environments are defined as those which are located close to the ice front of a glacier, ice cap, or ice sheet [36]. It is important to understand that glaciers are melting over time due to climate change, and being located in tropical zones exacerbates the thaw situation [37]. Meltwater from glaciers carries relatively large amounts of silt and clay-sized particles in suspension when high temperatures occur in the tropical zone; these particles are then deposited into proglacial lakes [38]. It is important to identify the origin of meltwater, which comes from glaciers and snow cover in a proglacial environment; this is possible through imagery from Sentinel-2 MSI L2A using the band 20 (Figure 2).

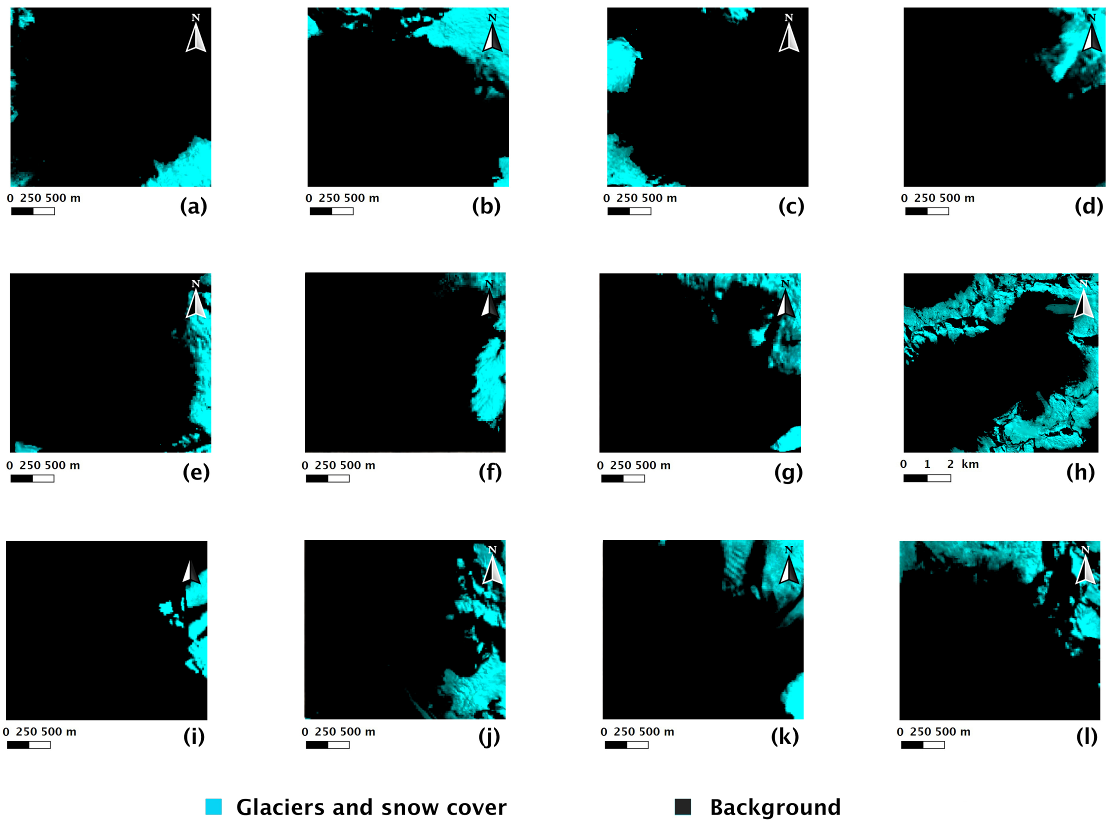

Figure 2. Glacier and snow cover from band 20 in Sentinel-2 MSI L2A at: (**a**) Allicocha, (**b**) Arhuaycocha, (**c**) Cancaragá, (**d**) 513 & Cochca, (**e**) Huallcacocha, (**f**) Llaca, (**g**) Palcacocha, (**h**) Parón, (**i**) Rajucolta, (**j**) Safuna Alta, (**k**) Tullpacocha, (**l**) Yanaraju.

Meltwater from glaciers that is the origin of a proglacial lake interacts with sedimentation influenced by climatic, glacial, and fluvial factors [39].

Sediments can be charged with radon, then radon flux will constantly interact with the tropical proglacial environment; this combination is an option to notice large turbulent flow from the impact of avalanches. Turbulent flows are present in tropical proglacial environments (Figure 3) with very close glaciers; this characteristic can be noticed with the band 20 from Sentinel-2 MSI L2A in overlap with another layer.

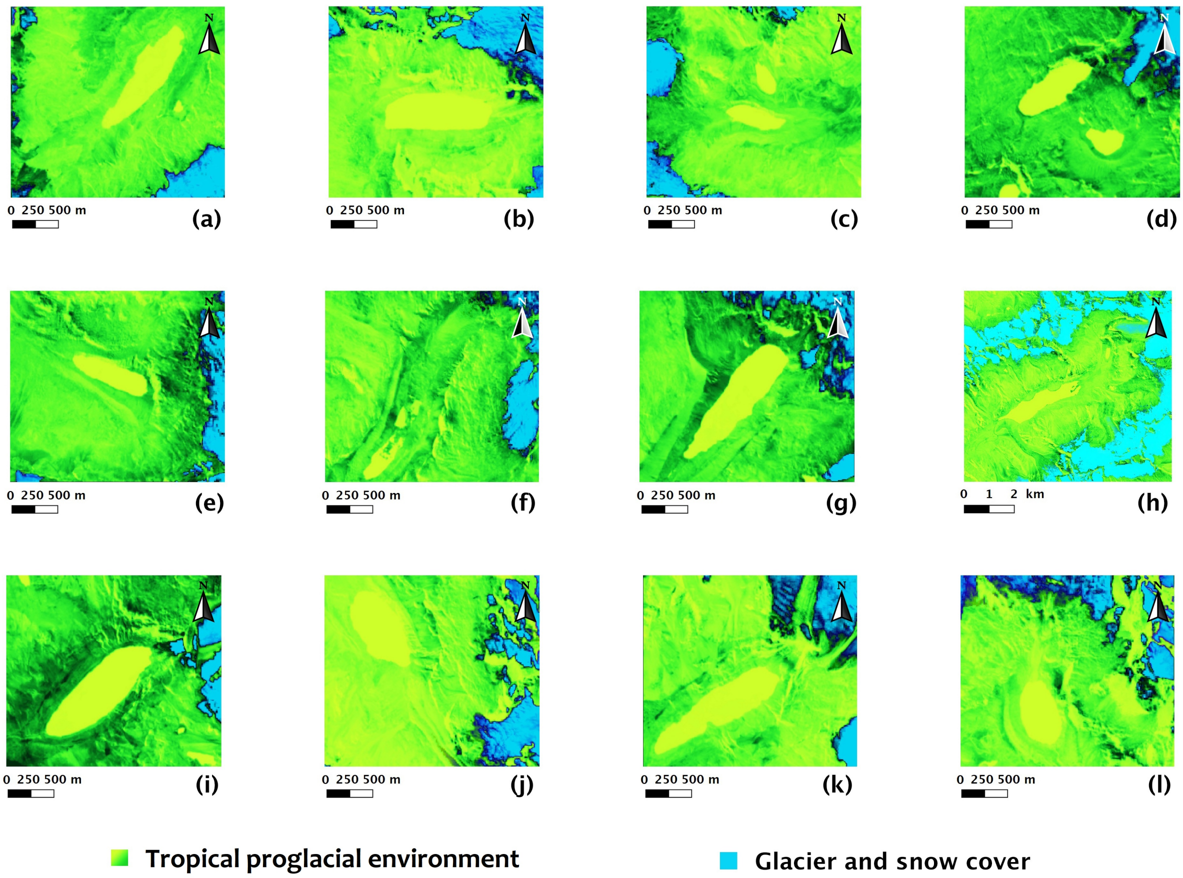

Figure 3. Glacier and snow cover from band 20 from Sentinel-2 MSI L2A, 2019–2020, with the tropical proglacial environment at: (**a**) Allicocha, (**b**) Arhuaycocha, (**c**) Cancaragá, (**d**) 513 & Cochca, (**e**) Huallcacocha, (**f**) Llaca, (**g**) Palcacocha, (**h**) Parón, (**i**) Rajucolta, (**j**) Safuna Alta, (**k**) Tullpacocha, (**l**) Yanaraju.

2.4. Palcacocha

The proglacial environment Palcacocha is in front of two glaciers, Palcaraju (6274 m.a.s.l.) and Pucaranra (6156 m.a.s.l.), which create a volume of water that generates the proglacial lake Palcacocha, which has a history of having suffered GLOFs; consequently, GLOF hazards have been a problem for the capital city of the Ancash region, Huaraz, for many years [40]. Glaciers in the western and eastern cordilleras of Peru generally underwent a very slow retreat between the 1950s and 1970s [41]. Throughout history, the largest GLOFs in the city of Huaraz are: On 13 December 1941, when a dam failed and a GLOF happened, Huaraz suffered great losses [42]; and on 31 May 1970, the cause was a 7.9-magnitude earthquake with disastrous effects [43]. In addition, another GLOF that caused secondary construction effects occurred in 2003, when there was a warning of flood danger, but it did not cause damage to nearby cities [44]. Currently, the proglacial Lake Palcacocha (Figure 4) is one of the main water resources for Huaraz, since its waters are partially captured to supply drinking water to the people of Huaraz; therefore, any geodynamic event that affects the quality of the proglacial waters in Lake Palcacocha will greatly affect the drinking water supply of Huaraz.

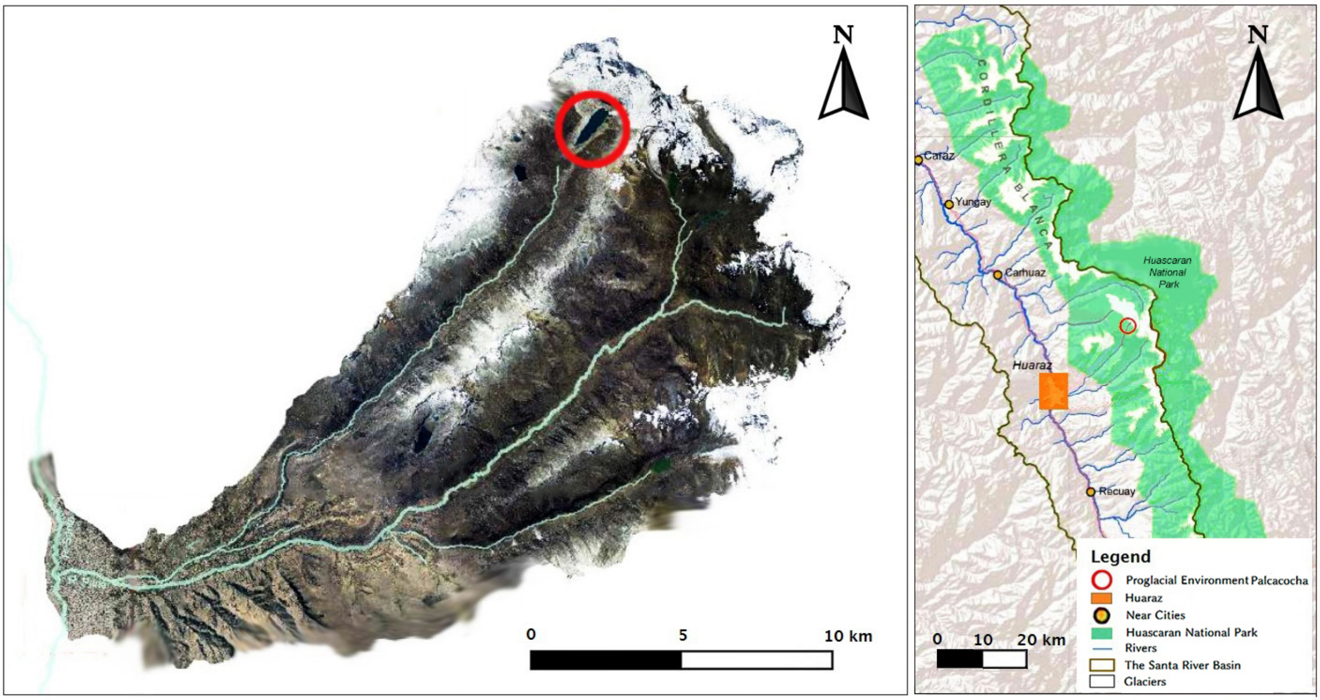

Figure 4. Location of proglacial environment Palcacocha, in reference to Huaraz.

2.5. Geology

The tropical glaciers of the Cordillera Blanca have played host to some of the most significant mass movements ever recorded in both the world and Peru; many proglacial lakes formed in this mountain range have natural dikes made of moraine material, which, if they collapse, would present a risk for the cities located downstream of the lagoon. The Cordillera Blanca is home to a significant number of tropical glaciers.

Most of the debris flows are caused by moraines breaking, many of which contained proglacial lakes; this created a problem for populations that are located downstream of tropical glaciers that generate large volumes of water, such as Huaraz, which is vulnerable to a flood event that may originate from the proglacial lake Palcacocha.

Alluvial deposits—The alluvial deposit is southwest of proglacial lake Palcacocha and forms an alluvial fan. It comprises the dragging and deposition of detrital material that originated from numerous discharges from the proglacial lake; one of these outbursts led to the rupture of the frontal moraine dike on 13 December 1941.

Moraines deposits—The moraines in the study area date to the Holocene (0.01 Ma); these deposits result from the action and retreat of glaciers during the ice ages. The hallmarks of moraines include their lack of stratification and their lack of significant consolidation. The composition of high mountain slopes is primarily granite, and there exists a difference between the frontal and lateral slopes; the lateral slope on the west has granite moraines deposits, while the lateral slope on the east is slate moraines deposits (Figure 5), finding high radon concentrations since uranium is more prevalent in the granite in the tropical proglacial environment.

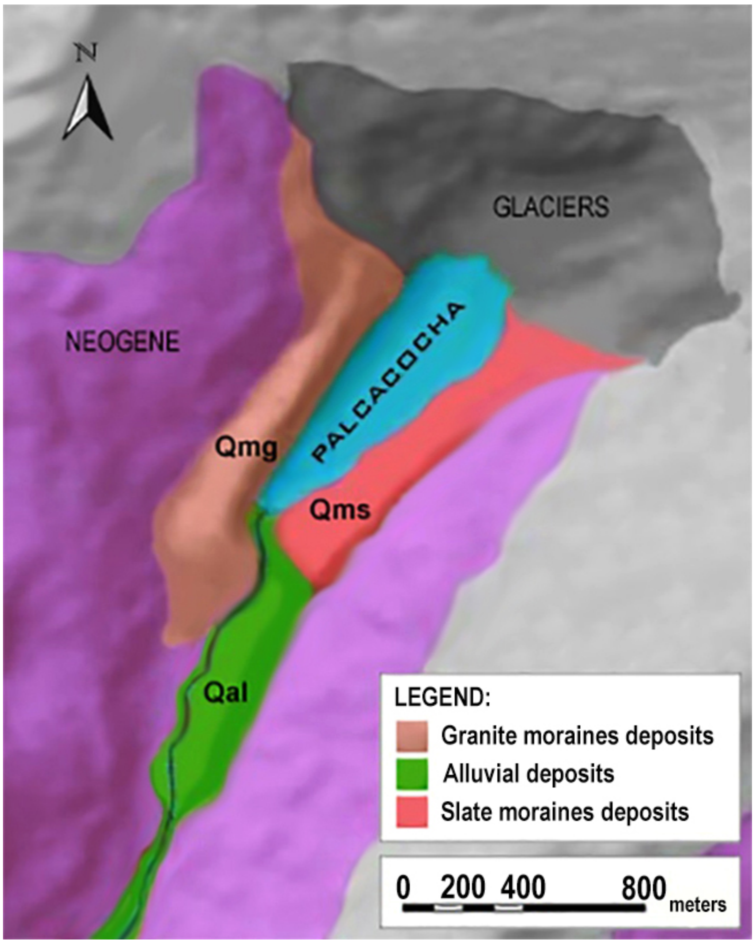

Figure 5. Local geology map of the proglacial environment Palcacocha.

3. Methodology

Satellite images provide evidence of changes in the territories due to both anthropogenic and natural causes. When a glacier generates meltwater for a new lake, is possible to identify with optical imagery collected over time [45]; this study used band 20 of the Sentinel-2 data in a cryosphere zone to obtain the highest quality imagery to detect the proglacial environment [46]. The multispectral imagery on board the Copernicus program's Sentinel-2 offers optimized bands for this task: Multi-Spectral Instrument, Level-2A (L2A), efficient use of bands such as blue (band 2), green (band 3), red (band 4), near-infrared (band 8), and a snow probability map (band 20) with 10-m spatial resolution [47]. With a dry season from May to September and a wet season from October to April, the climate of the proglacial environment Palcacocha exhibits a particular seasonality that should be taken into account when gathering data about the proglacial environment. The oscillation of the inner-tropic convergence zone regulates seasonality [48]. The best free tool for thematic mapping is high-resolution Sentinel-2 imagery, which is good for classifying land use and land cover [49].

3.1. Image Processing

To get data from Sentinel-2 MSI L2A, we select the zone through the cloud computing platform, Google Earth Engine (GEE), which has a collection of recent images from the Sentinel missions. Using image data from 2020 to 2022, we can find the proglacial environment of Palcacocha and to avoid imagery with clouds, encode the cloud mask in GEE to have imagery of the water body. The cloud computing platform GEE archived Sentinel-2 MSI L2A image data [50]. Bands from Sentinel-2 MSI L2A have a wide range of applications in many cryosphere zones, especially for glaciers and the proglacial environment where we use band 20 to detect glaciers and snow cover [51]. GEE's automatic methods help select the exact imagery of glaciers in the tropical zone and a specific tropical proglacial environment in Peru [52]. GEE, with the appropriate encoding for the objectives of identifying a tropical proglacial environment [53] and generating images using the Snow Probability Map (MSK_SNWPRB) to identify the tropical proglacial environment associated with the 10-m resolution data set that is presented in some bands of Sentinel-2 MSI L2A [54], is a great way to understand the relationship between water and ice. SNAP can calculate a useful index for the proglacial environments, the Normalized Difference Water Index, which is adapted for ice ($NDWI_{ice}$). It reflects the blue band that is relatively high in glacial environments, including in the tropical zone [55]. Based on remote sensing about optical imagery for recognizing proglacial lakes with the calculation of the $NDWI_{ice}$, described as

$$NDWI_{ice} = \frac{BLUE - RED}{BLUE + RED} \quad (1)$$

where $BLUE$ is the blue band (band 2 for Sentinel-2) and RED denotes the red band (band 4 for Sentinel-2).

3.2. Determination of Hot Spot for Radon Concentration in the Proglacial Environment

Finding the right area to install the collecting system for continuous radon measurements is known since it is near the proglacial lake, located by $NDWI_{ice}$, where the ice avalanches impact and create turbulence. Since Radon is a naturally occurring radioactive natural gas that is colorless, tasteless, and odorless [56]; different instruments and techniques are available for radon concentration detection and quantification [57]. An outstanding instrument for measuring radon is the RadonEye+ device, used in such a way that the device is more in contact with the measurement point. Additionally, its cylindrical shape greatly helps to collect more significant measurements, although being a cylinder, it is important to take 10 min for the air to stabilize inside the chamber. The RadonEye+ is a pulsed ion chamber type device with the following specifications: "RadonEye+ is a real-time smart radon detector which has a high sensitivity of 0.5 cpm/pCi/l, about 20–30 times more than conventional radon detectors by FTLAB's high stable circuit technology. RadonEye+ can measure up to 9700 Bq/m^3 of radon. Its first reliable data out time is below 60 min from measurement start. Furthermore, the accuracy is <10% at 10 pCi/l. The accuracy and precision specs were tested by the KTL (Korea Testing Laboratory, administered by the KOREAN government). RD200M is a radon sensing module for OEM supply". Radon concentration varies over time: shared daily cycles, local signals of several hours and several days, and shared annual and semi-annual periodic signals [58]. There are also lightweight instruments for measuring radon concentration [59] that are optimal for the proglacial environment and can support extreme cold events: The version RadonEye Plus2 additionally has Bluetooth connectivity, humidity, temperature measurements, and IoT technology. RadonEye Plus2 device was tested for this study in proglacial environments at elevations of more than 4566 m, and it worked normally.

The selected point hot spot is one where there are high radon concentrations; through point measurements such as Figure 6, it is recorded that a contained point where there is turbulent flow is helpful to the extent that it will show us high radon concentrations at present waves due to ice avalanche impacts, then a point contained in the perimeter of the proglacial lake (hot spot) is selected, in which through the collector system for continuous radon measurements (Figure 7), since RadonEye Plus2 has implemented IoT, which helps with monitoring radon concentrations and collecting radon concentration measurement data in real-time [60].

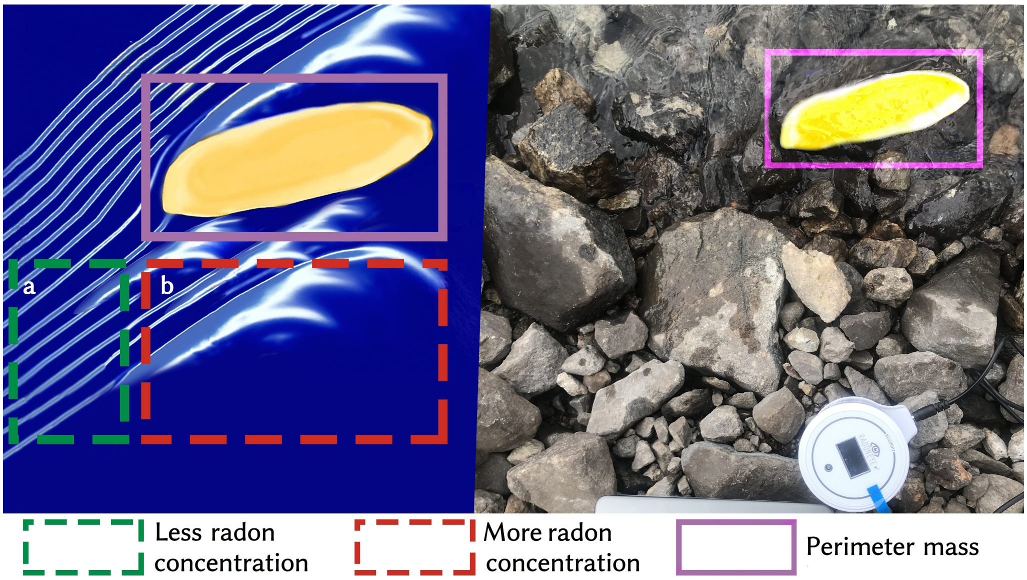

Figure 6. Interaction scenario with a perimeter mass of the proglacial lake. (a) Laminar flow: when particles move in parallel layers, or sheets, without invading the path of the other particles; in this situation, the radon concentration tends to be low. (b) Turbulent flow: when there are constant fluctuations in the flow and the particles invade the path of adjacent particles, mixing and moving randomly; in this situation, the radon concentration tends to be high.

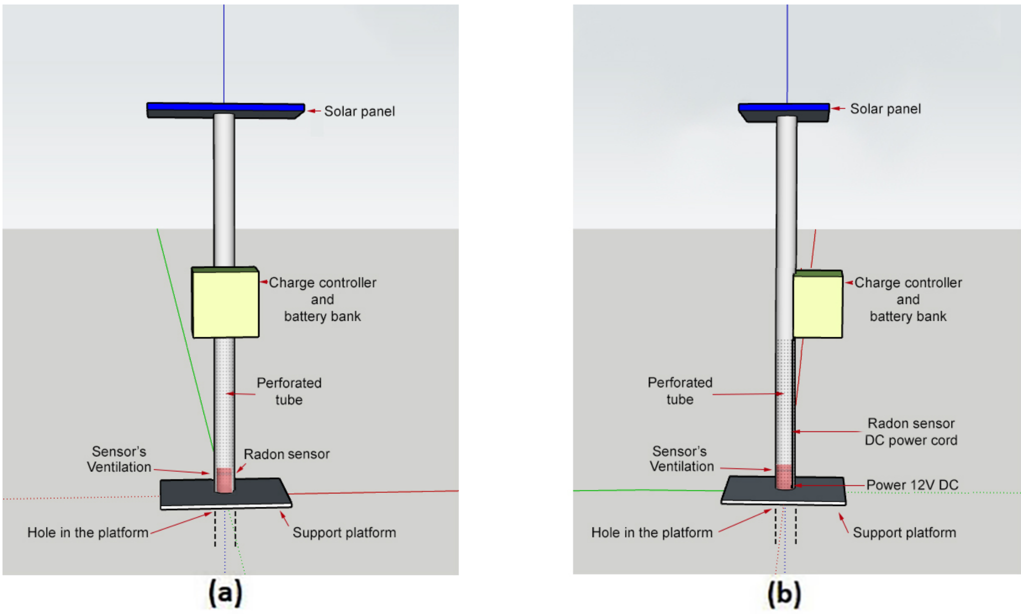

Figure 7. The collector system for continuous radon measurements. (**a**) Front view of the Collecting System for Radon EyePlus2. (**b**) Profile view of the collector system, including RadonEye Plus2's DC power cable conditioning.

In a proglacial environment, there are various interactions that cause different flows. Slow melting usually generates laminar flow; when there are impacts on the environment, as is the case when a glacial mass detaches or an avalanche occurs, then a turbulent flow is generated in the proglacial lake. There is still no single theory that provides predictability for a series of situations involving turbulent flow [61]. Analyzing this phenomenon even through physical experiments is a great challenge because of the need to include sensors or other flow observation tools, which can cause interference in the behavior of the fluid [62], and also require a hot spot. High radon concentrations are usually located at the perimeter of a proglacial lake where there is more interaction between sediments and rocks with meltwater. For radon concentration measurements across time in the tropical proglacial environment where the proglacial lake Palcacocha is located, having a characteristic hot spot located near the proglacial lake is important because that is frequently where a turbulent flow will happen. It is also where the concentration of radon has oscillatory behavior with high concentrations mainly generated by the ice avalanches from tropical glaciers (Figure 8) that impact the proglacial lake.

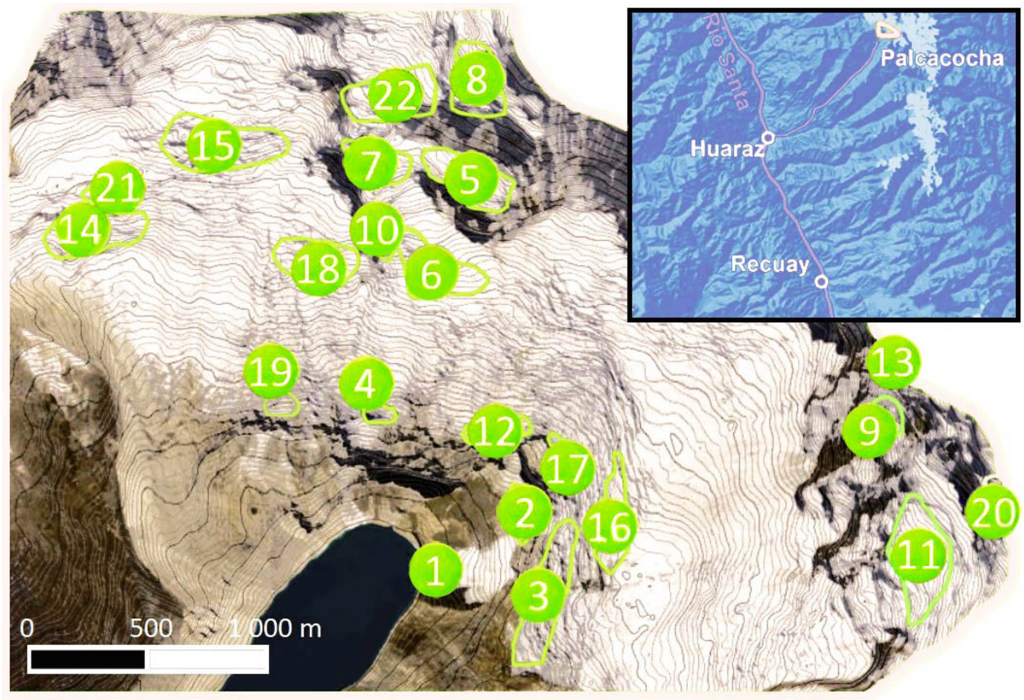

Figure 8. Unstable blocks of glacier mass close to the proglacial lake Palcacocha.

In the hot spot, the collection system is conditioned for continuous radon measurements, characterized by having a solar panel with its respective charge controller and battery bank to supply DC power for the operation of the radon sensor during 24 h a day, the radon sensor is located inside the tube that, in turn, supports the system since the sensor is in contact with the ground through a hole in the support platform; additionally, it has vertical ventilation. Table 2 analyzes each block numerated of glacier mass about mean slopes in Figure 8.

3.3. Radon Concentration in the Tropical Proglacial Environment

Glaciers located between the tropics can be analyzed from the point of view of radon concentrations. Since flux levels in any environment will have oscillatory behavior [63], interactions between a proglacial lake and tropical glaciers with many fluxes are of increasing concern for freshwater environmental management; however, there is often not enough data to characterize whether radon-222 is present in these environments, which can greatly help [64]. Noble gas degassing is more common than the ex-solution of water and other major gas phases acting as carriers of gaseous species, showing the main cause for radon occurrence [65] is meltwater supplied by tropical glaciers having natural radioactive elements. The most promising is precisely radon [66], which is a promising tracer in proglacial lakes that are stored in meltwater discharge [67]. Radon concentration is not static and is usually affected by atmospheric turbulence [68]; movements that involve turbulent flows have the potential to increase the concentration of radon in the air as ambient temperatures rise around water bodies, a frequent situation in tropical proglacial environments [69]. In this environment, the location of its corresponding proglacial lake is essential to identifying hot spots with high concentrations of radon in the area; locations of the ice water body using the $NDWI_{ice}$ is the index that can identify meltwater features [70]. In a tropical proglacial environment, it is possible to find radon concentration values that decrease; in this and other cases, we use this formula which expresses the limit value:

$$C(x) = \lim_{x \to \delta} \mid C_{Rn} \pm x \mid, \quad \delta > 0 \tag{2}$$

where C_{Rn} is the radon concentration and δ is value close to x generated by RadonEye Plus2.

3.4. Susceptibility of the Tropical Proglacial Environment

Global temperatures will continue to rise and will have a big impact on the cryosphere, where climate change is a threat to glaciers [71]. This threat is even more pronounced for the tropical proglacial environment; the melting of tropical glaciers is a response to global climate change whose consequence is the increase in proglacial lake volume and even the formation of new lakes [72]. Sediments in a proglacial lake with many impacts of ice avalanches are an important source for identifying susceptibility [73]. Figure 4 shows many scenarios in a tropical proglacial environment but is important to analyze the ones that have many ice avalanches that frequently impact a proglacial lake, as is the case of the proglacial lake Palcacocha that has impacts of ice avalanches that results in turbulent flow and consequently movement with sediments and changes in radon concentrations. In addition to the radon concentrations that vary due to the impacts of ice avalanches, in order to calculate the susceptibility of the area, it is also important to have data on the unstable blocks of glacier mass and their respective slopes; these are the origins of impacts to the proglacial lake [74]. We know that unstable blocks of ice form part of the glacier, so we perform a local analysis to exclude all remaining areas that are not connected to glacier ice. Glacier fluctuations are used to separate flat glacial forefields through multi-temporal change detection analysis [75].

Block volume and mean slope are represented as:

$$tan\alpha = 1.111 - 0.118Log_{10}(V) \tag{3}$$

where α is the mean slope, and V is the block volume of glacier mass in cubic meters [75].

The unstable blocks of glacier mass that impact the proglacial lake Palcacocha come mainly from the deglaciation of the glaciers Palcaraju and Pucaranra (Figure 8). Tropical glaciers tend to lose mass as a consequence of climate change, causing them to generate unstable ice blocks, the main agents of susceptibility in a proglacial lake. At proglacial lake Palcacocha, there are ice avalanches originating from the unstable ice blocks. The defined spatial distribution of mean daily surface velocities concerning elevation shows the zones where it is possible to take points that tend to present unstable blocks of glacier mass, the points contained in the tropical glaciers. In Figure 8, we see the points that have unstable blocks of glacier mass.

There are also cases of ice avalanches with low average slopes and extraordinarily large volumes which generate debris-laden flows [76] because climate change defragments a glacier. Figure 8 is generated principally by melting, which occurs frequently in Palcacocha's glaciers and has the potential of generating a GLOF.

Table 2. Blocks of glacier mass with mean slopes.

Block	Volume (m^3)	$1.111 - 0.118 \cdot \mathrm{Log}_{10} V$	Mean Slope
1	185,565.68	0.49	26.07°
2	354,002.21	0.47	24.52°
3	339,487.87	0.46	24.62°
4	239,807.95	0.48	25.46°
5	411,099.35	0.45	24.16°
6	665,229.59	0.42	22.97°
7	125,613.68	0.51	26.99°
8	34,258.28	0.58	29.94°
9	194,130.25	0.49	25.97°
10	125,613.68	0.51	26.99°
11	765,101.52	0.42	22.62°
12	205,549.67	0.48	25.83°
13	45,677.70	0.56	29.30°
14	548,132.41	0.43	23.45°
15	765,101.56	0.42	22.62°
16	708,004.43	0.42	22.82°
17	22,518.76	0.60	30.85°
18	479,615.90	0.44	23.78°
19	159,871.97	0.50	26.43°
20	68,515.97	0.54	28.39°
21	171,291.40	0.49	26.26°
22	37,033.23	0.57	29.77°

4. Results

The sensor for continuous radon measurements: RadonEye Plus2 operated continuously in Rn point (Figure 9). Figure 10 shows an important meltwater location (calculated with $NDWI_{ice}$) concentrated in the proglacial lake where it is susceptible to GLOF, as an antecedent of the one that happened in 1941 in Huaraz. Analyzing the lithology from imagery with *SWIR* and local geology information in tropical proglacial environments shows granite moraine deposits in light red and slate moraines in dark red.

From continuous measurement in Rn point; radon concentrations, temperature, and humidity, for the respective time series established in Figure 11. Radon is a gas that moves with the air, so it needs to be constantly monitored since tropical proglacial environments are affected by ice avalanches whose leading causes are climate change and the respective deglaciation.

The point for continuous measures is located at a longitude of −77.381698° and latitude of −9.397037°, the point called: Rn Point Figure 9 is where RadonEye Plus2 continuously collects at one-hour intervals; these continuous measurements were made between 28 March and 10 May 2022. If the tropical proglacial environment has glaciers very close with steep slopes that generate susceptibility, there will be ice avalanches. Tropical glaciers are efficiently located with MSK_SNWPRB from Sentinel-2 MSI L2A.

When ice avalanches impact the proglacial Lake Palcacocha, turbulent flow is produced, which causes the radon concentration to increase drastically [77]. The observation range of the graphs of Figure 11a–c has been considered, which involves the time series of radon, temperature, and humidity, respectively. We can see from Figure 12a,b that there is a relationship between radon and temperature (R^2 = 0.364) as well as between radon and humidity (R^2 = 0.469); the stronger in the tropical proglacial environment being radon with humidity.

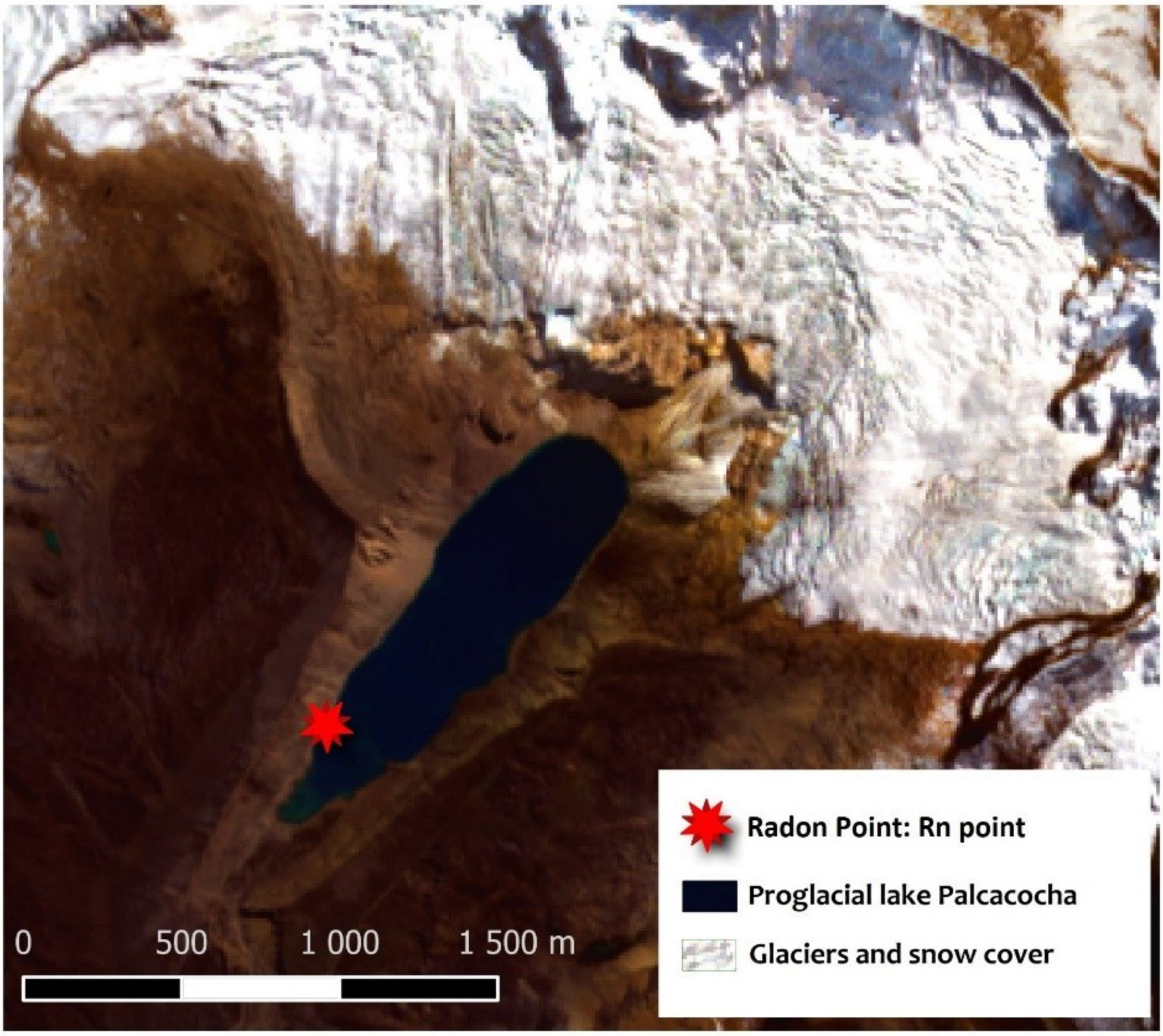

Figure 9. Location of the Rn point for continuous measurement of radon concentrations.

Table 3 presents the statistical parameters of radon concentration, temperature, and humidity for Rn point in the proglacial environment Palcacocha.

Table 3. Summary statistics of radon concentration, temperature, and humidity.

Parameter	N	AM	SD	Min	Max	Median	GM
Radon (Bq/m^3)	1048	1674.63	1205.06	2	6502	1351.5	1272.14
Temperature (°C)	1048	8.98	7.26	0.5	29	5.5	6.34
Humidity (%)	1048	73	8	45	99	74	72

N—number of observations; AM—arithmetic mean; SD—standard deviation; GM—geometric mean.

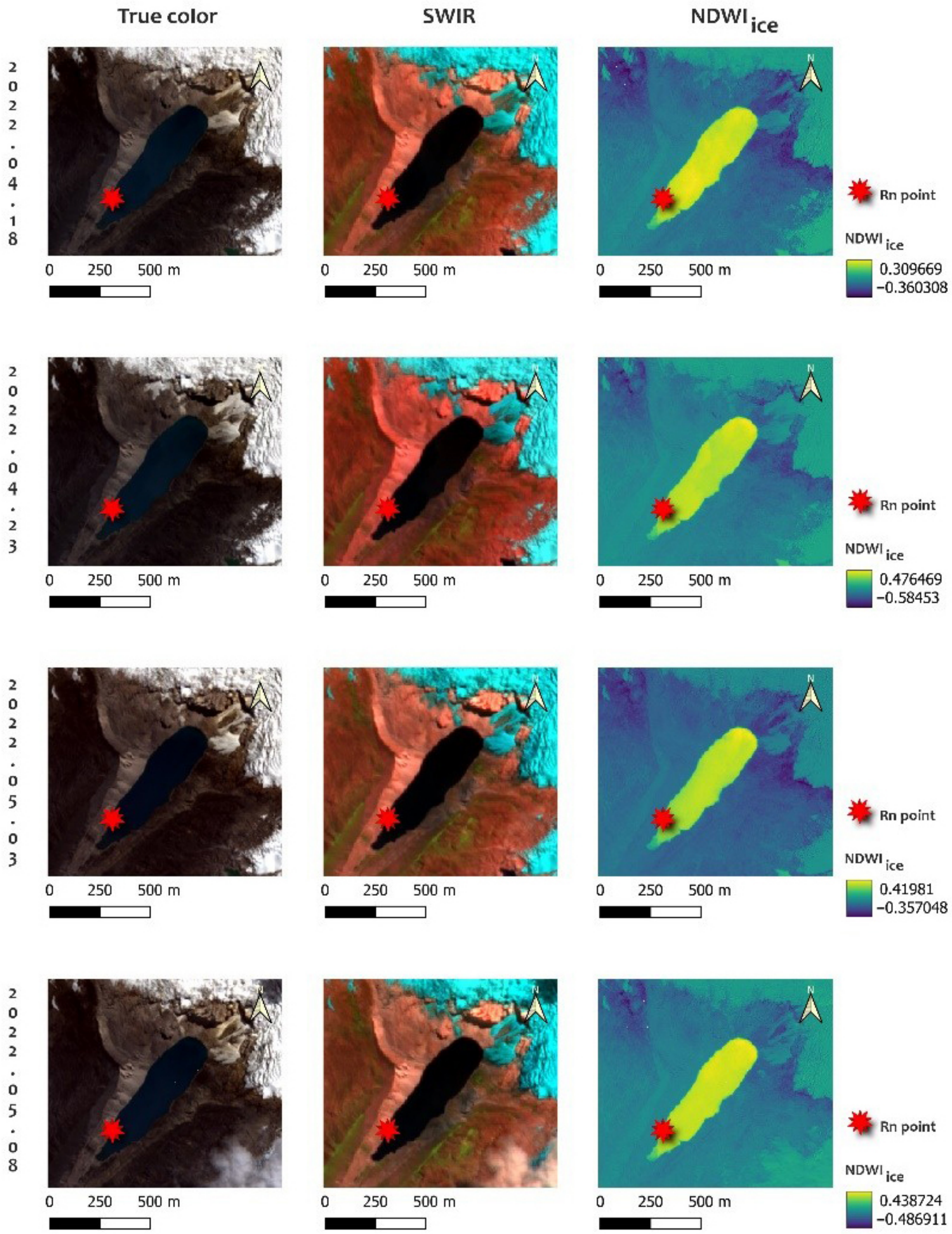

Figure 10. Measurements in the Rn point in the tropical proglacial environment.

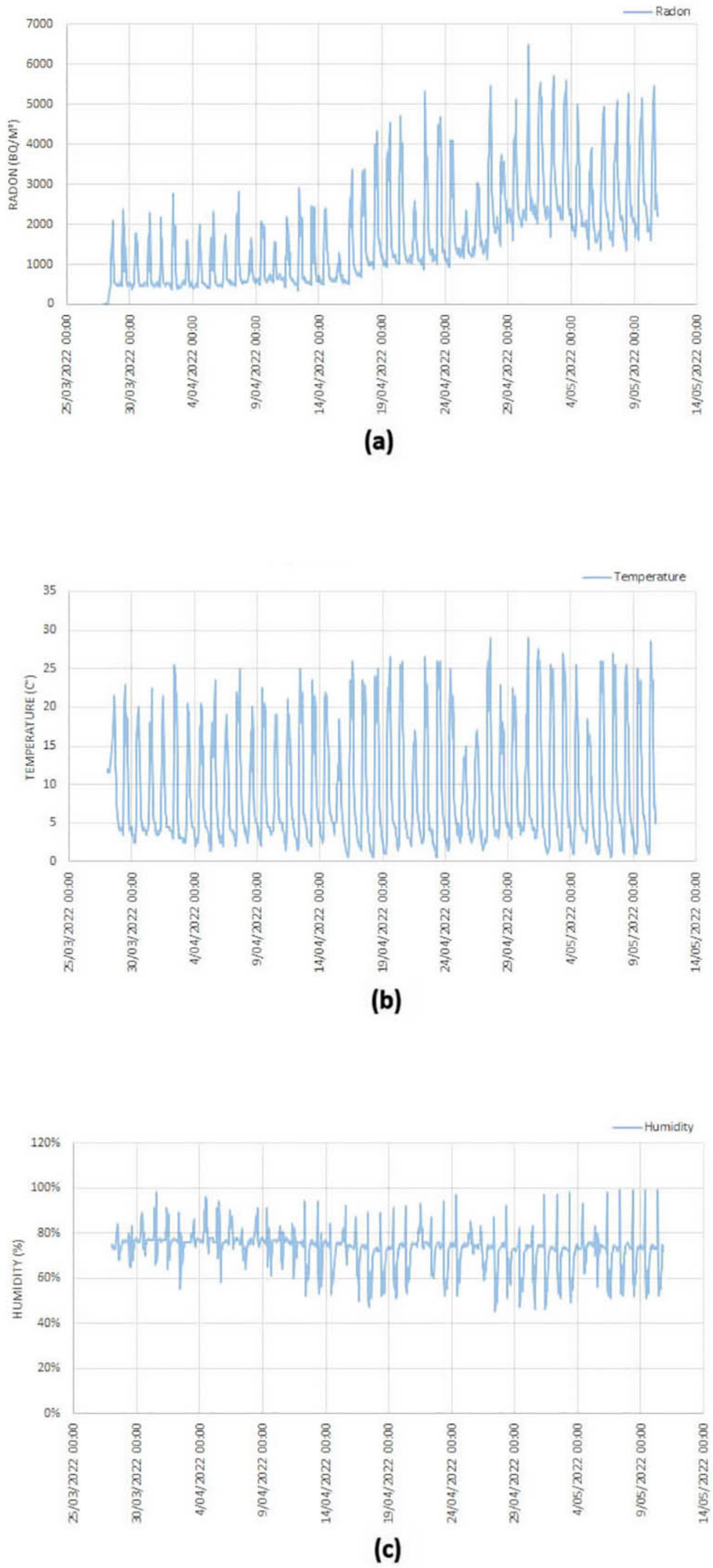

Figure 11. Time series. (**a**) Radon time series. (**b**) Temperature time series. (**c**) Humidity Time series.

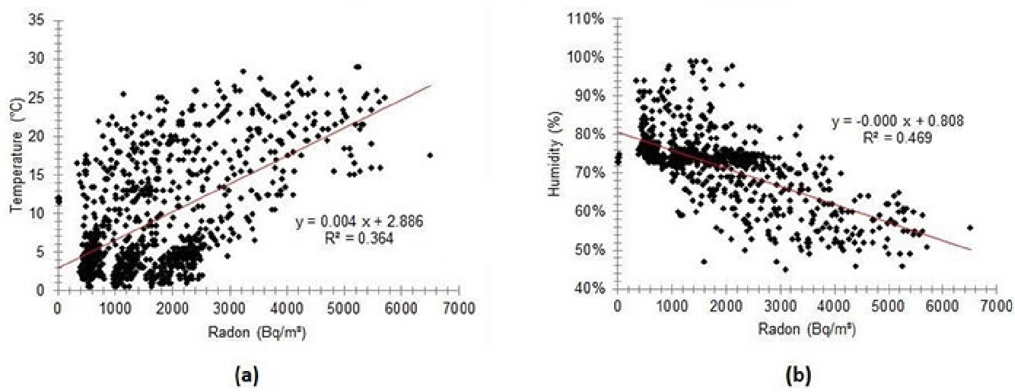

Figure 12. Scatter plot. (**a**) Radon relationship with temperature (R^2 = 0.364). (**b**) Radon relationship with humidity (R^2 = 0.469).

5. Discussion

The R Square in Table 4 is for radon with temperature (R^2 = 0.364), and this relationship was shown to have highly significant F (0.44×10^{-104} in Table 5). The R Square in Table 6 is for radon with humidity (R^2 = 0.469), with F (0.436×10^{-145} in Table 7).

All the coefficients are in a significant level of p-value less than 0.001.

Table 4. Regression statistics for radon and temperature.

Multiple R	R Square	Adjusted R Square	Standar Error	Observations
0.6037	0.3645	0.3639	5.7919	1048

Table 5. Summary of the ANOVA for radon and temperature.

	df	SS	MS	F	Significance F
Regression	1	20,125.337	20,125.337	599.923	0.44×10^{-104}
Residual	1046	35,089.701	33.547		
Total	1047	55,212.038			
	Coefficients	**Standard Error**	**t Stat**	**p-Value**	
Intercept	2.886	0.306	9.420	0.279×10^{-19}	
Radon (Bq/m³)	0.004	0.149×10^{-3}	24.493	0.44×10^{-104}	

Table 6. Regression statistics for radon and humidity.

Multiple R	R Square	Adjusted R Square	Standar Error	Observations
0.6851	0.4693	0.4688	0.0605	1048

Table 7. Summary of the ANOVA for radon and humidity.

	df	SS	MS	F	Significance F
Regression	1	3.382	3.382	925.089	0.436×10^{-145}
Residual	1046	3.824	0.004		
Total	1047	7.207			
	Coefficients	**Standard Error**	**t Stat**	**p-Value**	
Intercept	0.808	0.003	252.627	0	
Radon (Bq/m³)	-0.472×10^{-4}	0.155×10^{-5}	−30.415	0.461×10^{-145}	

For the linear trend about radon and temperature by ANOVA, the *p*-value of 0.279×10^{-19} is favorable for the coefficient 2.886. Regarding the *p*-value of 0.44×10^{-104}, it is favorable for the coefficient 0.004 of radon.

For the linear trend about radon and humidity by ANOVA, the *p*-value of 0 is highly favorable for the coefficient 0.808. Regarding the *p*-value of 0.461×10^{-145}, it is favorable for the coefficient -0.472×10^{-4} of radon.

A tropical proglacial environment is characterized as being located close to at least one glacier located in a tropical environment; being susceptible to climate change, then since radon is present in significant concentrations, it is necessary to understand its relationships for both radon with temperature (Tables 4 and 5) and radon with humidity (Tables 6 and 7). Regarding optical imagery, Sentinel-2 MSI (Multi-Spectral Instrument Level-2A) has a specific band for mapping snow probability, and is a highly accurate tool for locating tropical glaciers. Due to melting, a proglacial lake tends to generate entropy in its immediate surroundings, and if the glaciers have steep slopes, this will generate a large flow with impacts of ice avalanches. Additionally, it is essential to know the lithological mapping, since radon is the product of natural radioactive decay; therefore, after knowing the lithology, optical images provide, through *SWIR*, the recognition of granite moraine deposits and slate moraine moraines in the proglacial environment Palcacocha. $NDWI_{ice}$ allows us to accurately determine the extent of the proglacial lake since rock and sediments interact with the meltwater at the perimeter, where the significant radon concentrations are located; it is there that the continuous measurement device RadonEye Plus2 is located (Rn Point) and the simultaneous measurements of radon, temperature and humidity provide the information for generating a time series (Figure 11a–c). The proglacial Lake Palcacocha receives impacts due to the detachment of glacial mass caused largely by climate change; radon measurements must be made simultaneously with the temperature, and the results show a relationship of $R^2 = 0.364$ (Figure 12a). This is unusual in an environment close to a mountainous cryosphere and is explained by the fact that it is located in a tropical zone. In the specific case of the proglacial environment of Lake Palcacocha, the strongest relationship is that of humidity to radon: $R^2 = 0.469$ (Figure 12b); when humidity rises, radon concentrations fall, showing in scenarios with precipitation where radon has low concentrations. Radon measurements in the study area show that a proglacial environment whose geographic location is in the Earth's tropical zone is susceptible since radon values fluctuate (Figure 12) with temperature and humidity; radon concentrations tend to change in a turbulent flow in response to movements and effects presented by the impacts of ice avalanches. As a consequence, the concentrations of radon exist and interact in the tropical proglacial environment [78], and high detachment of glacial mass causes impacts of ice avalanches in the tropical proglacial environment, generating vibrations which cause a high concentration of radon. Radon measurements definitely are an important source of data since the proglacial environment Palcacocha has a history of seismic events, being that Peru is a country at risk of earthquakes, which can cause a GLOF like the one in Ancash in the earthquake of 1970 [79]. Movements produced by internal or external geodynamics directly affect proglacial environments, especially those found in the tropical zone and having a high slope; there, a glacier mass detachment or moraine collapse will create a GLOF scenario and therefore an imminent flood in nearby vulnerable cities [80].

6. Conclusions

In this study, to prevent potential damage and losses by GLOFs, we analyzed a tropical proglacial environment. The identification of the study zone is efficient through MSK_SNWPRB from Sentinel-2 MSI L2A; for the proglacial lake, we used $NDWI_{ice}$ and *SWIR* to define the moraines. For radon measurements, the selection of the measurement point is more efficient on the perimeter of the proglacial lake, where, through the RadonEye Plus2, the continuous measurements of radon over time with simultaneous readings with temperature ($R^2 = 0.364$) and humidity ($R^2 = 0.469$) are evidenced.

Regarding exposure to radon, knowledge of radon's dangers must be widely conveyed on the site since radon levels, as found, are substantially greater than those suggested by the WHO (100 Bq/m^3) and are beyond the 300 Bq/m^3 level suggested by the EURATOM Regulation 2013/59. People in a proglacial environment with sites of a preponderance of granite moraine deposits must take appropriate action.

Due to the zone's earthquake hazard, further research in proglacial environments for implementation of an early warning system with IoT coupling radon measurements to establish a resilient zone against natural hazards by debris flow studies in these environments should be continued in the future. Furthermore, supporting and implementing radon reduction, mitigation, and remediation efforts is necessary.

Author Contributions: Conceptualization, D.A.G.-T., M.M.-Z. and Y.T.; methodology, D.A.G.-T., M.M.-Z. and Y.T.; investigation, D.A.G.-T., M.M.-Z. and Y.T.; software D.A.G.-T., M.M.-Z. and Y.T.; data curation, D.A.G.-T., M.M.-Z. and Y.T.; writing—original draft, D.A.G.-T.; visualization, D.A.G.-T. and M.M.-Z.; supervision, M.M.-Z. and Y.T.; project administration, D.A.G.-T.; funding acquisition, D.A.G.-T. All authors have read and agreed to the published version of the manuscript.

Funding: This study has been supported by Institute for Research on Glaciers and Mountain Ecosystems (INAIGEM).

Data Availability Statement: The data presented in this study are available on request from the corresponding author.

Acknowledgments: This research was partly supported by National Institute for Research on Glaciers and Mountain Ecosystems (INAIGEM), Office of Information and Knowledge Management—DIGC about "Agreement for assistance and subsidy for scientific and academic research thesis". Olga A. Tadeo-Loli, Antonio F. García-Huesa, Antonio García-Laurencio, Yolvi E. García-Tadeo, Luis M. Coral-Jamanca, Daniel Martínez-Castro and José A. Herrera-Quispe are gratefully acknowledged. The accuracy identification of tropical proglacial environment was supported partly by Sentinel-2 trough GEE and processed with SNAP 8.0.0.

Conflicts of Interest: The authors declare no conflict of interest.

References

1. Carrivick, J.L.; Tweed, F.S. A Global Assessment of the Societal Impacts of Glacier Outburst Floods. *Glob. Planet. Chang.* **2016**, *144*, 1–16. [CrossRef]
2. Ruano-Raviña, A.; Quindós-Poncela, L.; Sainz Fernández, C.; Barros-Dios, J.M. Radón interior y salud pública en España. Tiempo para la acción. *Gac. Sanit.* **2014**, *28*, 439–441. [CrossRef] [PubMed]
3. Kies, A.; Hengesch, O.; Tosheva, Z.; Nawrot, A.P.; Jania, J. Overview on Radon Measurements in Arctic Glacier Waters. *Cryosph. Discuss.* **2015**, *9*, 2013–2052. [CrossRef]
4. Stanley, F.K.T.; Irvine, J.L.; Jacques, W.R.; Salgia, S.R.; Innes, D.G.; Winquist, B.D.; Torr, D.; Brenner, D.R.; Goodarzi, A.A. Radon Exposure Is Rising Steadily within the Modern North American Residential Environment, and Is Increasingly Uniform across Seasons. *Sci. Rep.* **2019**, *9*, 18472. [CrossRef]
5. Linhoff, B.S.; Charette, M.A.; Nienow, P.W.; Wadham, J.L.; Tedstone, A.J.; Cowton, T. Utility of 222Rn as a Passive Tracer of Subglacial Distributed System Drainage. *Earth Planet. Sci. Lett.* **2017**, *462*, 180–188. [CrossRef]
6. Akbari, K.; Mahmoudi, J.; Ghanbari, M. Influence of Indoor Air Conditions on Radon Concentration in a Detached House. *J. Environ. Radioact.* **2013**, *116*, 166–173. [CrossRef]
7. Rabi, R.; Oufni, L. Study of Radon Dispersion in Typical Dwelling Using CFD Modeling Combined with Passive-Active Measurements. *Radiat. Phys. Chem. Oxf. Engl.* **2017**, *139*, 40–48. [CrossRef]
8. Martin, I.M. Radon Gas Intensity Variation from April to July 2018 in São José Dos Campos, Brazil Region. *Glob. J. Eng. Sci. Res.* **2018**, *5*, 90–96. [CrossRef]
9. Aydar, E.; Diker, C. Carcinogen Soil Radon Enrichment in a Geothermal Area: Case of Güzelçamlı-Davutlar District of Aydın City, Western Turkey. *Ecotoxicol. Environ. Saf.* **2021**, *208*, 111466. [CrossRef]
10. Shrestha, B.B.; Nakagawa, H.; Kawaike, K.; Zhang, H. Glacial and Sediment Hazards in the Rolwaling Valley, Nepal. *Int. J. Eros. Contr. Eng.* **2012**, *5*, 123–133. [CrossRef]
11. Zhu, Z.; Wang, S.; Woodcock, C.E. Improvement and Expansion of the Fmask Algorithm: Cloud, Cloud Shadow, and Snow Detection for Landsats 4–7, 8, and Sentinel 2 Images. *Remote Sens. Environ.* **2015**, *159*, 269–277. [CrossRef]
12. Wang, Y.; Su, J.; Zhai, X.; Meng, F.; Liu, C. Snow Coverage Mapping by Learning from Sentinel-2 Satellite Multi-Spectral Images via Machine Learning Algorithms. *Remote Sens.* **2022**, *14*, 782. [CrossRef]

13. Paul, F.; Rastner, P.; Azzoni, R.S.; Diolaiuti, G.; Fugazza, D.; Le Bris, R.; Nemec, J.; Rabatel, A.; Ramusovic, M.; Schwaizer, G.; et al. Glacier Shrinkage in the Alps Continues Unabated as Revealed by a New Glacier Inventory from Sentinel-2. *Earth Syst. Sci. Data* **2020**, *12*, 1805–1821. [CrossRef]
14. Verma, P.; Kumar Ghosh, S. Classification of Glacial Lakes Using Integrated Approach of DFPS Technique and Gradient Analysis Using Sentinel 2A Data. *Geocarto Int.* **2019**, *34*, 1075–1088. [CrossRef]
15. Hollstein, A.; Segl, K.; Guanter, L.; Brell, M.; Enesco, M. Ready-to-Use Methods for the Detection of Clouds, Cirrus, Snow, Shadow, Water and Clear Sky Pixels in Sentinel-2 MSI Images. *Remote Sens.* **2016**, *8*, 666. [CrossRef]
16. Zharko, V.O.; Bartalev, S.A.; Sidorenkov, V.M. Forest Growing Stock Volume Estimation Using Optical Remote Sensing over Snow-Covered Ground: A Case Study for Sentinel-2 Data and the Russian Southern Taiga Region. *Remote Sens. Lett.* **2020**, *11*, 677–686. [CrossRef]
17. Gilfedder, B.S.; Frei, S.; Hofmann, H.; Cartwright, I. Groundwater Discharge to Wetlands Driven by Storm and Flood Events: Quantification Using Continuous Radon-222 and Electrical Conductivity Measurements and Dynamic Mass-Balance Modelling. *Geochim. Cosmochim. Acta* **2015**, *165*, 161–177. [CrossRef]
18. Peano, G.; Vigna, B.; Villavecchia, E.; Agnesod, G. Radon Exchange Dynamics in a Karst System Investigated by Radon Continuous Measurements in Water: First Results. *Radiat. Prot. Dosim.* **2011**, *145*, 173–177. [CrossRef]
19. Burnett, W.C.; Wattayakorn, G.; Supcharoen, R.; Sioudom, K.; Kum, V.; Chanyotha, S.; Kritsananuwat, R. Groundwater Discharge and Phosphorus Dynamics in a Flood-Pulse System: Tonle Sap Lake, Cambodia. *J. Hydrol.* **2017**, *549*, 79–91. [CrossRef]
20. Lázaro, L.V.; López Herrera, M.E.; Pereyra, P.; Fernández, D.P.; Pérez, B.; Rojas, J.; Sajo-Bohus, L. Measurement of Radon in Soils of Lima City—Peru during the Period 2016–2017. *Earth Sci. Res. J.* **2019**, *23*, 171–183. [CrossRef]
21. Vuille, M.; Francou, B.; Wagnon, P.; Juen, I.; Kaser, G.; Mark, B.G.; Bradley, R.S. Climate Change and Tropical Andean Glaciers: Past, Present and Future. *Earth Sci. Rev.* **2008**, *89*, 79–96. [CrossRef]
22. Mark, B.G.; Seltzer, G.O. Tropical Glacier Meltwater Contribution to Stream Discharge: A Case Study in the Cordillera Blanca, Peru. *J. Glaciol.* **2003**, *49*, 271–281. [CrossRef]
23. Kaser, G.; Juen, I.; Georges, C.; Gómez, J.; Tamayo, W. The Impact of Glaciers on the Runoff and the Reconstruction of Mass Balance History from Hydrological Data in the Tropical Cordillera Blanca, Perú. *J. Hydrol.* **2003**, *282*, 130–144. [CrossRef]
24. Somos-Valenzuela, M.A.; Chisolm, R.E.; Rivas, D.S.; Portocarrero, C.; McKinney, D.C. Modeling a Glacial Lake Outburst Flood Process Chain: The Case of Lake Palcacocha and Huaraz, Peru. *Hydrol. Earth Syst. Sci.* **2016**, *20*, 2519–2543. [CrossRef]
25. Veettil, K. Global Disappearance of Tropical Mountain Glaciers: Observations, Causes, and Challenges. *Geoscience* **2019**, *9*, 196. [CrossRef]
26. Vuille, M.; Carey, M.; Huggel, C.; Buytaert, W.; Rabatel, A.; Jacobsen, D.; Soruco, A.; Villacis, M.; Yarleque, C.; Elison Timm, O.; et al. Rapid Decline of Snow and Ice in the Tropical Andes—Impacts, Uncertainties and Challenges Ahead. *Earth Sci. Rev.* **2018**, *176*, 195–213. [CrossRef]
27. Pouyaud, B.; Zapata, M.; Yerren, J.; Gomez, J.; Rosas, G.; Suarez, W.; Ribstein, P. Avenir Des Ressources En Eau Glaciaire de La Cordillère Blanche/On the Future of the Water Resources from Glacier Melting in the Cordillera Blanca, Peru. *Hydrol. Sci. J.* **2005**, *50*, 999. [CrossRef]
28. Kaser, G. A Review of the Modern Fluctuations of Tropical Glaciers. *Glob. Planet. Chang.* **1999**, *22*, 93–103. [CrossRef]
29. Emmer, A.; Vilímek, V.; Klimeš, J.; Cochachin, A. Glacier Retreat, Lakes Development and Associated Natural Hazards in Cordilera Blanca, Peru. In *Landslides in Cold Regions in the Context of Climate Change*; Springer International Publishing: Cham, Switzerland, 2014; pp. 231–252. [CrossRef]
30. Baraer, M.; Mark, B.G.; McKenzie, J.M.; Condom, T.; Bury, J.; Huh, K.-I.; Portocarrero, C.; Gómez, J.; Rathay, S. Glacier Recession and Water Resources in Peru's Cordillera Blanca. *J. Glaciol.* **2012**, *58*, 134–150. [CrossRef]
31. Drenkhan, F.; Huggel, C.; Guardamino, L.; Haeberli, W. Managing Risks and Future Options from New Lakes in the Deglaciating Andes of Peru: The Example of the Vilcanota-Urubamba Basin. *Sci. Total Environ.* **2019**, *665*, 465–483. [CrossRef]
32. Hanshaw, M.N.; Bookhagen, B. Glacial Areas, Lake Areas, and Snow Lines from 1975 to 2012: Status of the Cordillera Vilcanota, Including the Quelccaya Ice Cap, Northern Central Andes, Peru. *Cryosphere* **2014**, *8*, 359–376. [CrossRef]
33. Shugar, D.H.; Burr, A.; Haritashya, U.K.; Kargel, J.S.; Watson, C.S.; Kennedy, M.C.; Bevington, A.R.; Betts, R.A.; Harrison, S.; Strattman, K. Rapid Worldwide Growth of Glacial Lakes since 1990. *Nat. Clim. Chang.* **2020**, *10*, 939–945. [CrossRef]
34. Reznichenko, N.V.; Davies, T.R.H.; Alexander, D.J. Effects of Rock Avalanches on Glacier Behaviour and Moraine Formation. *Geomorphology* **2011**, *132*, 327–338. [CrossRef]
35. Read, L.K.; McKinney, D.C. *Addressing Water Availability and Climate Change Issues in the Cordillera Blanca, Peru through Technical Analysis and Community Building Strategies*; Center for Research in Water Resources, University of Texas at Austin: Austin, TX, USA, 2010. Available online: http://hdl.handle.net/2152/10899 (accessed on 8 February 2023).
36. Slaymaker, O. Criteria to Distinguish Between Periglacial, Proglacial and Paraglacial Environments. *Quaest. Geogr.* **2011**, *30*, 85–94. [CrossRef]
37. Rabatel, A.; Francou, B.; Soruco, A.; Gomez, J.; Cáceres, B.; Ceballos, J.L.; Basantes, R.; Vuille, M.; Sicart, J.-E.; Huggel, C.; et al. Current State of Glaciers in the Tropical Andes: A Multi-Century Perspective on Glacier Evolution and Climate Change. *Cryosphere* **2013**, *7*, 81–102. [CrossRef]
38. Eawag, A.F.L.; Eicher, U.; Siegenthaler, U.; Birks, H.J.B. Late-Glacial Climatic Oscillations as Recorded in Swiss Lake Sediments. *J. Quat. Sci.* **1992**, *7*, 187–204. [CrossRef]

39. Leemann, A.; Niessen, F. Holocene Glacial Activity and Climatic Variations in the Swiss Alps: Reconstructing a Continuous Record from proglacial Lake Sediments. *Holocene* **1994**, *4*, 259–268. [CrossRef]
40. Huggel, C.; Carey, M.; Emmer, A.; Frey, H.; Walker-Crawford, N.; Wallimann-Helmer, I. Anthropogenic Climate Change and Glacier Lake Outburst Flood Risk: Local and Global Drivers and Responsibilities for the Case of Lake Palcacocha, Peru. *Nat. Hazards Earth Syst. Sci.* **2020**, *20*, 2175–2193. [CrossRef]
41. Hastenrath, S.; Ames, A. Recession of Yanamarey Glacier in Cordillera Blanca, Peru, during the 20th Century. *J. Glaciol.* **1995**, *41*, 191–196. [CrossRef]
42. Vilímek, V.; Zapata, M. L.; Klimeš, J.; Patzelt, Z.; Santillán, N. Influence of Glacial Retreat on Natural Hazards of the Palcacocha Lake Area, Peru. *Landslides* **2005**, *2*, 107–115. [CrossRef]
43. Xu, C.; Xu, X.; Yao, X.; Dai, F. Three (Nearly) Complete Inventories of Landslides Triggered by the May 12, 2008 Wenchuan Mw 7.9 Earthquake of China and Their Spatial Distribution Statistical Analysis. *Landslides* **2014**, *11*, 441–461. [CrossRef]
44. Klimeš, J.; Novotný, J.; Novotná, I.; de Urries, B.J.; Vilímek, V.; Emmer, A.; Strozzi, T.; Kusák, M.; Rapre, A.C.; Hartvich, F.; et al. Landslides in Moraines as Triggers of Glacial Lake Outburst Floods: Example from Palcacocha Lake (Cordillera Blanca, Peru). *Landslides* **2016**, *13*, 1461–1477. [CrossRef]
45. Tom, M.; Prabha, R.; Wu, T.; Baltsavias, E.; Leal-Taixé, L.; Schindler, K. Ice Monitoring in Swiss Lakes from Optical Satellites and Webcams Using Machine Learning. *Remote Sens.* **2020**, *12*, 3555. [CrossRef]
46. Main-Knorn, M.; Pflug, B.; Louis, J.; Debaecker, V.; Müller-Wilm, U.; Gascon, F. Sen2Cor for Sentinel-2. In *Image and Signal Processing for Remote Sensing XXIII*; Bruzzone, L., Bovolo, F., Benediktsson, J.A., Eds.; SPIE Remote Sensing: Warsaw, Poland, 2017. [CrossRef]
47. Zhu, K.; Ghobrial, T.; Loewen, M. Exploration of Google earth engine for monitoring river ice. In Proceedings of the 21st Workshop on the Hydraulics of Ice Covered Rivers, Saskatoon, SK, Canada, 29 August–1 September 2021.
48. Kos, A.; Amann, F.; Strozzi, T.; Osten, J.; Wellmann, F.; Jalali, M.; Dufresne, A. The Surface Velocity Response of a Tropical Glacier to Intra and Inter Annual Forcing, Cordillera Blanca, Peru. *Remote Sens.* **2021**, *13*, 2694. [CrossRef]
49. Chymyrov, A.; Betz, F.; Baibagyshov, E.; Kurban, A.; Cyffka, B.; Halik, U. Floodplain Forest Mapping with Sentinel-2 Imagery: Case Study of Naryn River, Kyrgyzstan. In *Vegetation of Central Asia and Environs*; Springer International Publishing: Cham, Switzerland, 2018; pp. 335–347. [CrossRef]
50. Chastain, R.; Housman, I.; Goldstein, J.; Finco, M.; Tenneson, K. Empirical Cross Sensor Comparison of Sentinel-2A and 2B MSI, Landsat-8 OLI, and Landsat-7 ETM+ Top of Atmosphere Spectral Characteristics over the Conterminous United States. *Remote Sens. Environ.* **2019**, *221*, 274–285. [CrossRef]
51. Wang, Q.; Shi, W.; Li, Z.; Atkinson, P.M. Fusion of Sentinel-2 Images. *Remote Sens. Environ.* **2016**, *187*, 241–252. [CrossRef]
52. Carrasco, L.; O'Neil, A.; Morton, R.; Rowland, C. Evaluating Combinations of Temporally Aggregated Sentinel-1, Sentinel-2 and Landsat 8 for Land Cover Mapping with Google Earth Engine. *Remote Sens.* **2019**, *11*, 288. [CrossRef]
53. Zhang, M.; Huang, H.; Li, Z.; Hackman, K.O.; Liu, C.; Andriamiarisoa, R.L.; Ny Aina Nomenjanahary Raherivelo, T.; Li, Y.; Gong, P. Automatic High-Resolution Land Cover Production in Madagascar Using Sentinel-2 Time Series, Tile-Based Image Classification and Google Earth Engine. *Remote Sens.* **2020**, *12*, 3663. [CrossRef]
54. Corbane, C.; Politis, P.; Kempeneers, P.; Simonetti, D.; Soille, P.; Burger, A.; Pesaresi, M.; Sabo, F.; Syrris, V.; Kemper, T. A Global Cloud Free Pixel- Based Image Composite from Sentinel-2 Data. *Data Brief* **2020**, *31*, 105737. [CrossRef]
55. Yang, K.; Smith, L.C. Supraglacial Streams on the Greenland Ice Sheet Delineated from Combined Spectral—Shape Information in High-Resolution Satellite Imagery. *IEEE Geosci. Remote Sens. Lett.* **2013**, *10*, 801–805. [CrossRef]
56. Feng, T.; Lu, X. Natural Radioactivity, Radon Exhalation Rate and Radiation Dose of Fly Ash Used as Building Materials in Xiangyang, China. *Indoor Built Environ.* **2016**, *25*, 626–634. [CrossRef]
57. Elísio, S.; Peralta, L. Development of a Low-Cost Monitor for Radon Detection in Air. *Nucl. Instrum. Methods Phys. Res. A* **2020**, *969*, 164033. [CrossRef]
58. Dimitrova, I.; Georgiev, S.; Mitev, K.; Todorov, V.; Dutsov, C.; Sabot, B. Study of the Performance and Time Response of the RadonEye Plus2 Continuous Radon Monitor. *Measurement (London)* **2023**, *207*, 112409. [CrossRef]
59. Martín-Martín, A.; Gutiérrez-Villanueva, J.L.; Muñoz, J.M.; García-Talavera, M.; Adamiec, G.; Iñiguez, M.P. Radon Measurements with a PIN Photodiode. *Appl. Radiat. Isot* **2006**, *64*, 1287–1290. [CrossRef] [PubMed]
60. Sá, J.P.; Branco, P.T.B.S.; Alvim-Ferraz, M.C.M.; Martins, F.G.; Sousa, S.I. V. Radon in Indoor Air: Towards Continuous Monitoring. *Sustainability* **2022**, *14*, 1529. [CrossRef]
61. Leith, C.E. Theoretical Skill of Monte Carlo Forecasts. *Mon. Weather Rev.* **1974**, *102*, 409–418. Available online: https://journals.ametsoc.org/view/journals/mwre/102/6/1520-0493_1974_102_0409_tsomcf_2_0_co_2.xml (accessed on 15 December 2022). [CrossRef]
62. Deng, Z.; He, C.; Liu, Y. Deep Neural Network-Based Strategy for Optimal Sensor Placement in Data Assimilation of Turbulent Flow. *Phys. Fluids* **2021**, *33*, 025119. [CrossRef]
63. Wilkening, M.H. Radon 222 Concentrations in the Convective Patterns of a Mountain Environment. *J. Geophys. Res.* **1970**, *75*, 1733–1740. [CrossRef]
64. Arnoux, M.; Gibert-Brunet, E.; Barbecot, F.; Guillon, S.; Gibson, J.; Noret, A. Interactions between Groundwater and Seasonally Ice-covered Lakes: Using Water Stable Isotopes and Radon-222 Multilayer Mass Balance Models. *Hydrol. Process.* **2017**, *31*, 2566–2581. [CrossRef]

65. Gauthier, P.-J.; Condomines, M.; Hammouda, T. An Experimental Investigation of Radon Diffusion in an Anhydrous Andesitic Melt at Atmospheric Pressure: Implications for Radon Degassing from Erupting Magmas. *Geochim. Cosmochim. Acta* **1999**, *63*, 645–656. [CrossRef]
66. Kies, A.; Nawrot, A.; Tosheva, Z.; Jania, J. Natural Radioactive Isotopes in Glacier Meltwater Studies. *Geochem. J.* **2011**, *45*, 423–429. [CrossRef]
67. Bhatia, M.P.; Das, S.B.; Kujawinski, E.B.; Henderson, P.; Burke, A.; Charette, M.A. Seasonal Evolution of Water Contributions to Discharge from a Greenland Outlet Glacier: Insight from a New Isotope-Mixing Model. *J. Glaciol.* **2011**, *57*, 929–941. [CrossRef]
68. Kobayashi, Y.; Yasuoka, Y.; Omori, Y.; Nagahama, H.; Sanada, T.; Muto, J.; Suzuki, T.; Homma, Y.; Ihara, H.; Kubota, K.; et al. Annual Variation in the Atmospheric Radon Concentration in Japan. *J. Environ. Radioact.* **2015**, *146*, 110–118. [CrossRef] [PubMed]
69. Smetanová, I.; Holý, K.; Müllerová, M.; Polášková, A. The Effect of Meteorological Parameters on Radon Concentration in Borehole Air and Water. *J. Radioanal. Nucl. Chem.* **2010**, *283*, 101–109. [CrossRef]
70. Hu, J.; Huang, H.; Chi, Z.; Cheng, X.; Wei, Z.; Chen, P.; Xu, X.; Qi, S.; Xu, Y.; Zheng, Y. Distribution and Evolution of Supraglacial Lakes in Greenland during the 2016–2018 Melt Seasons. *Remote Sens.* **2021**, *14*, 55. [CrossRef]
71. Chevallier, P.; Pouyaud, B.; Suarez, W.; Condom, T. Climate Change Threats to Environment in the Tropical Andes: Glaciers and Water Resources. *Reg. Environ. Chang.* **2011**, *11*, 179–187. [CrossRef]
72. Khadka, N.; Chen, X.; Nie, Y.; Thakuri, S.; Zheng, G.; Zhang, G. Evaluation of Glacial Lake Outburst Flood Susceptibility Using Multi-Criteria Assessment Framework in Mahalangur Himalaya. *Front. Earth Sci.* **2021**, *8*, 601288. [CrossRef]
73. Dearing, J.A.; Elner, J.K.; Happey-Wood, C.M. Recent Sediment Flux and Erosional Processes in a Welsh Upland Lake-Catchment Based on Magnetic Susceptibility Measurements. *Quat. Res.* **1981**, *16*, 356–372. [CrossRef]
74. Iribarren Anacona, P.; Norton, K.P.; Mackintosh, A. Moraine-Dammed Lake Failures in Patagonia and Assessment of Outburst Susceptibility in the Baker Basin. *Nat. Hazards Earth Syst. Sci.* **2014**, *14*, 3243–3259. [CrossRef]
75. Paul, F.; Huggel, C.; Kääb, A. Combining Satellite Multispectral Image Data and a Digital Elevation Model for Mapping Debris-Covered Glaciers. *Remote Sens. Environ.* **2004**, *89*, 510–518. [CrossRef]
76. Kääb, A.; Jacquemart, M.; Gilbert, A.; Leinss, S.; Girod, L.; Huggel, C.; Falaschi, D.; Ugalde, F.; Petrakov, D.; Chernomorets, S.; et al. Sudden Large-Volume Detachments of Low-Angle Mountain Glaciers—More Frequent than Thought? *Cryosphere* **2021**, *15*, 1751–1785. [CrossRef]
77. Chen, Y.; Hong, C.; Li, X.; Liu, Y.; Chen, Y.; Dai, X.; Wang, H.; Lin, D. Effect of Simulated Earthquake Loading on Radon Exhalation from Uranium Tailings Dam. *Environ. Sci. Pollut. Res. Int.* **2022**, *29*, 79434–79442. [CrossRef] [PubMed]
78. Dugan, H.A.; Gleeson, T.; Lamoureux, S.F.; Novakowski, K. Tracing Groundwater Discharge in a High Arctic Lake Using Radon-222. *Environ. Earth Sci.* **2012**, *66*, 1385–1392. [CrossRef]
79. Kuroiwa, J. Peru Sustainable (Resilient) Cities Programme 1998–2012. Its Application 2014–2021. *Procedia Econ. Financ.* **2014**, *18*, 408–415. [CrossRef]
80. Moulton, H.; Carey, M.; Huggel, C.; Motschmann, A. Narratives of Ice Loss: New Approaches to Shrinking Glaciers and Climate Change Adaptation. *Geoforum* **2021**, *125*, 47–56. [CrossRef]